LETTER

doi:10.1038/nature11567

Optical-field-induced current in dielectrics

Agustin Schiffrin[1]†, Tim Paasch-Colberg[1], Nicholas Karpowicz[1], Vadym Apalkov[2], Daniel Gerster[3], Sascha Mühlbrandt[1,3], Michael Korbman[1], Joachim Reichert[3], Martin Schultze[1,4], Simon Holzner[1], Johannes V. Barth[3], Reinhard Kienberger[1,3], Ralph Ernstorfer[1,3,5], Vladislav S. Yakovlev[1,4], Mark I. Stockman[2] & Ferenc Krausz[1,4]

The time it takes to switch on and off electric current determines the rate at which signals can be processed and sampled in modern information technology[1–4]. Field-effect transistors[1–3,5,6] are able to control currents at frequencies of the order of or higher than 100 gigahertz, but electric interconnects may hamper progress towards reaching the terahertz (10^{12} hertz) range. All-optical injection of currents through interfering photoexcitation pathways[7–10] or photoconductive switching of terahertz transients[11–16] has made it possible to control electric current on a subpicosecond timescale in semiconductors. Insulators have been deemed unsuitable for both methods, because of the need for either ultraviolet light or strong fields, which induce slow damage or ultrafast breakdown[17–20], respectively. Here we report the feasibility of electric signal manipulation in a dielectric. A few-cycle optical waveform reversibly increases—free from breakdown—the a.c. conductivity of amorphous silicon dioxide (fused silica) by more than 18 orders of magnitude within 1 femtosecond, allowing electric currents to be driven, directed and switched by the instantaneous light field. Our work opens the way to extending electronic signal processing and high-speed metrology into the petahertz (10^{15} hertz) domain.

Three basic types of solid—metals, semiconductors and dielectrics—fundamentally differ in their reaction to an applied electric field. Metals respond to a small field with a current linearly proportional to it. This implies a strong screening that prevents high fields and charge density gradients from forming inside metals, which makes it fundamentally difficult to control their responses. By contrast, semiconductors, in which there is a relatively small but non-zero energy gap, Δ_g, between the valence and conduction bands, allow electric fields to penetrate and charge gradients to build up. This forms the basis of contemporary digital electronics[1–3,21]. Dielectrics, with their large bandgap and conduction and valence band widths, offer the fastest response. However, because of their reaction to applied fields (that is, extremely low conductivity at low fields and breakdown at high fields[17–20]), they have been thought to be unsuitable for electronic signal processing in field-effect devices. Here we demonstrate that a strong, few-cycle optical field is capable of transforming the dielectric into a state of highly increased polarizability, allowing optical currents to flow and resulting in macroscopic charge separation that is detectable in an external circuit.

In our experiments, we exposed a fused silica[22] sample ($\Delta_g \approx 9$ eV and conduction band width $\Delta_c \approx 10$ eV) to a strong, waveform-controlled, few-cycle field $F_i(t)$ with a photon energy of $\hbar\omega_L \approx 1.7$ eV (where $\hbar$ denotes Planck's constant divided by 2π and ω_L is the carrier angular frequency of the optical field), which transforms the dielectric into an optically conducting state, that is, injects carriers. We therefore refer to this field as the injection field. By carriers, we mean electrons in highly polarizable states at optical frequencies (rather than ones capable of conducting d.c. current, requiring delocalized electrons). Two unbiased gold electrodes collect the charge separated by the optical-field-induced current (Fig. 1a, Methods Summary and Supplementary Information). First, the applied external field $F_i(t) = F_0 f(t) \cos(\omega_L t + \varphi_{CE})$, with a controlled carrier-envelope phase (CEP) φ_{CE}, a sub-4-fs envelope $f(t)$ with $f(0) = 1$, and $F_0 \approx 1.7$ V Å^{-1}, was polarized perpendicularly to the metal–dielectric interface, along coordinate x, to drive the generated carriers towards the electrodes (Fig. 1a). Fig. 2 plots Q_P, the charge transferred through the ammeter shown in Fig. 1 during exposure to a single laser pulse, as a function of the change in φ_{CE} (Fig. 2a) and as a function of F_0 (Fig. 2b). The CEP of the laser pulse is shifted by $\Delta\varphi_{CE}$ on changing the

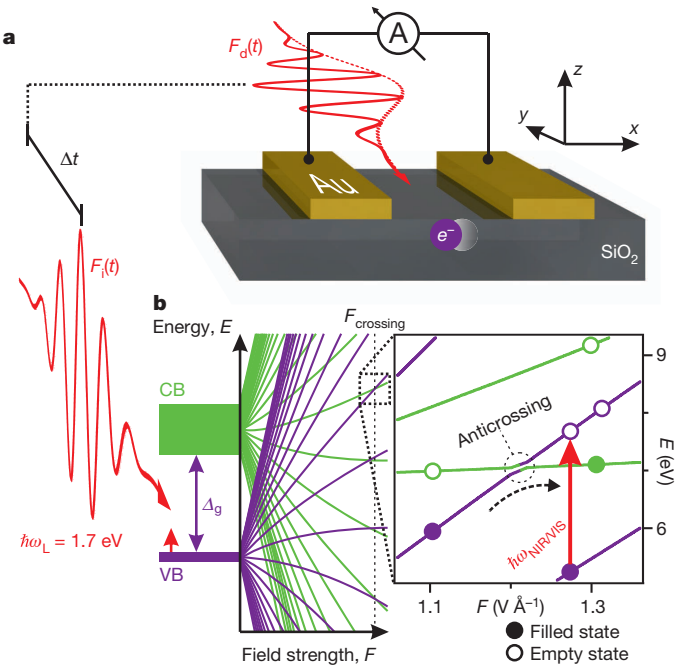

Figure 1 | Optical-field-induced conductivity and current control in a dielectric. **a**, Schematic of the metal–dielectric nanojunction. **b**, Schematic illustration of the adiabatic energy levels of the electronic states in the valence band (VB, purple) and conduction band (CB, green) of the dielectric under the influence of a static or slowly varying strong electric field. The eigenenergies fan out as the strength of the electric field increases, resulting in avoided crossings, that is, anticrossings (inset). At low fields, the valence band states are occupied, and the conduction band states are empty. As the field strength increases, the valence band and conduction band levels cross, but the respective Wannier–Stark states are localized at distant sites, and the anticrossings are passed diabatically (that is, the conduction band states remain unpopulated) until the field approaches or exceeds ~1 V Å^{-1}. At these field strengths, electrons may be promoted into the conduction band via Zener tunnelling, leaving the electron in the lower-energy state after the passage of the anticrossing (adiabatic transition, depicted by dashed arrow). The resultant unoccupied valence band states mediate strong single-photon resonances at visible/near-infrared angular frequencies $\omega_{NIR/VIS}$ within the valence band (red arrow). The emergence of these resonances results in a strong transient polarizability.

[1]Max-Planck-Institut für Quantenoptik, Hans-Kopfermann-Strasse 1, D-85748 Garching, Germany. [2]Department of Physics and Astronomy, Georgia State University, Atlanta, Georgia 30340, USA. [3]Physik-Department, Technische Universität München, James-Franck-Strasse, D-85748 Garching, Germany. [4]Fakultät für Physik, Ludwig-Maximilians-Universität, Am Coulombwall 1, D-85748 Garching, Germany. [5]Fritz-Haber-Institut der Max-Planck-Gesellschaft, Faradayweg 4–6, 14195 Berlin, Germany. †Present addresses: Department of Physics and Astronomy, University of British Columbia, Vancouver, British Columbia, V6T 1Z1 Canada; Quantum Matter Institute, University of British Columbia, Vancouver, British Columbia, V6T 1Z4 Canada.

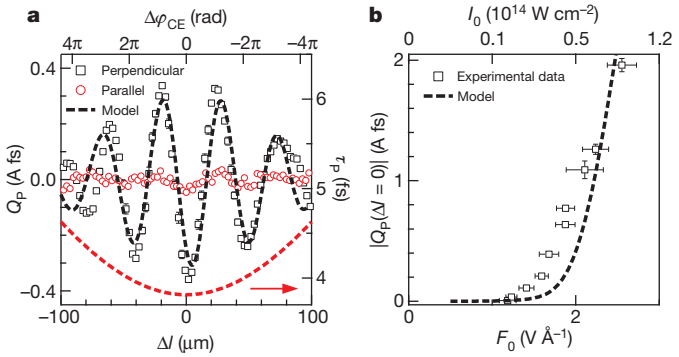

Figure 2 | Carrier-envelope-phase control and intensity dependence of optical-field-generated electric current in SiO_2. **a**, Plot of the φ_{CE}-dependent component of $Q_P(\Delta l)$ against the change, Δl, in the propagation length through a fused silica wedge with respect to the propagation length yielding the minimum pulse duration ($\Delta l = 0$), for polarizations perpendicular (along x; squares) and parallel (in the y–z plane; circles) to the metal–dielectric interface ($F_0 \approx 1.7$ V Å^{-1}). The data represent an average of several consecutively acquired values at a given value of Δl. Error bars show the standard deviation, and most are smaller than the size of the symbols representing the mean values of the data. The black dashed line shows the prediction of our quantum mechanical model. For the parallel polarization, the signal is suppressed by more than an order of magnitude. The residual signal is attributed to microscopic imperfections of the macroscopically plane metal–dielectric interface, which result in locations with a non-zero perpendicular component of the field. The red dashed line (right axis) depicts the change in pulse duration τ_P (full width at half maximum intensity) as a function of Δl, taking into account the group velocity dispersion of the visible/near-infrared pulse in the fused silica wedge. **b**, Plot of the maximum amplitude, $|Q_P(\Delta l = 0)|$, of the transferred charge against the peak amplitude, F_0, of the applied external field polarized along x: measurement (squares) and theoretical prediction (dashed line). For a given F_0 value, $|Q_P(\Delta l = 0)|$ is determined by fitting the most pronounced oscillation of $Q_P(\Delta l)$ (**a**, squares) with a sine function. The vertical error bars account for the standard deviation of such fit. Different values of F_0 correspond to different beam sizes. Data points have been normalized accordingly. F_0 is determined by monitoring the pulse energy and the laser beam waist at the focus, and the horizontal error bars quantify random fluctuations in these parameters. I_0 is the corresponding peak intensity of the optical pulse. Data from our model have been multiplied by the effective cross-section, A_{eff}, of the metal–dielectric interfaces confining the active volume of the dielectric (main text).

propagation length by Δl in a pair of thin, fused silica wedges[23] (Methods Summary and Supplementary Fig. 1).

We find that Q_P varies quasi-periodically with Δl. Its minimum at $\Delta l = 0$ turns into a maximum at $\Delta l = \pm \Delta l_{deph}$, with $\Delta l_{deph} = 23$ μm shifting[23] the CEP by $\Delta\varphi_{CE} = \pi$, which results in an approximate inversion of the optical waveform: $F_i(t, \Delta l_{deph}) \approx -F_i(t, 0)$. This reversal of Q_P and its order-of-magnitude reduction when $F_i(t)$ is polarized parallel to the metal–dielectric interface (that is, in the y–z plane) provide the first significant indication that this current is induced directly by the instantaneous light field. The maximum value of Q_P scales nearly exponentially with the field amplitude and reaches ~10^4 electrons before breakdown (Fig. 2b). This nonlinear dependence is responsible for the decay of $Q_P(\Delta l)$ with increasing Δl, as a consequence of dispersive pulse broadening.

To decouple the injection and driving processes, we irradiated the hybrid junction with two synchronized, orthogonally polarized fields. An injection field with a peak amplitude of $F_0^{(i)} \approx 2$ V Å^{-1} was polarized parallel to the electrode–insulator interface (that is, in the y–z plane) to prevent it from driving current through the circuit. This driving was accomplished by a weaker version of the same field, the drive field $F_d(t)$, which had an amplitude of $F_0^{(d)} \approx 0.2$ V Å^{-1} (Fig. 1a). The delay, Δt, between the peaks of $F_i(t)$ and $F_d(t)$ determines the timing of carrier injection with respect to the drive field and thereby controls the momentum that $F_d(t)$ transfers to the charge carriers. Fig. 3a shows Q_P versus Δt for the CEPs of the injection ($\varphi_{CE}^{(i)}$) and drive ($\varphi_{CE}^{(d)}$) pulses corresponding to one of the zero-crossings of Q_P near $\Delta l = 0$ in Fig. 2a. Such values of $\varphi_{CE}^{(i)}$ and $\varphi_{CE}^{(d)}$ are chosen to avoid a residual (background) current originating in any of the fields independently (Fig. 2a).

The transferred charge periodically changes its sign as a function of Δt, revealing two major current reversal cycles equal to the field oscillation cycle of $F_d(t)$ (Fig. 3a). The magnitude of the signal rapidly decays outside this few-femtosecond delay interval. Fig. 3b plots the result of the same measurement performed with an 'inverted' drive field, in which the field oscillations are reversed by shifting the CEP by $\Delta\varphi_{CE}^{(d)} = \pi$. For any value of Δt, the transferred charge is reversed with respect to its value at the same delay in Fig. 3a. This is exactly the behaviour we intuitively expect for a current driven directly by $F_d(t)$. The observed $Q_P(\Delta t)$ reflecting the oscillating behaviour of $F_d(t)$ provides compelling evidence that the light field governs the current that emerges from the dielectric medium and is measured in the external circuit. The transferred charge was also found to depend sensitively on the CEP of the injection field $\varphi_{CE}^{(i)}$ (Supplementary Fig. 7). This also corroborates the evidence that carrier injection is induced directly by the instantaneous field $F_i(t)$ rather than by effects governed by the cycle-averaged intensity. Experiments on free-standing electrodes kept under helium flux did not yield any φ_{CE}-dependent electronic signal under identical irradiation conditions (Supplementary Fig. 10), and so we identify the insulator as the primary source of current in our experiments.

Fig. 3c plots the electric field waveform of the drive pulse retrieved from attosecond streaking[24]. Such streaking experiments were performed in a parallel ultrahigh vacuum set-up independently from the light-field-induced current measurements and under identical laser conditions. The good correspondence between the solid lines in Fig. 3a and Fig. 3c suggests that the injected carriers sample the optical field with good fidelity. Carrier injection must therefore be substantially confined to a half-period, that is, to a time window of ~1 fs. This confinement is also indicative of a strong nonlinearity, in accordance with Fig. 2b.

To describe our observations theoretically, we calculate the current density, $j_x(t)$, generated in the bulk insulator along coordinate x by solving the time-dependent Schrödinger equation for a dielectric film with a thickness in the range 50–500 nm exposed to a strong optical field. We neglect the Coulomb interaction between the electrons, which is justified by the extremely short (~1 fs) timescale on which the processes occur. The time dependence of the applied electric fields is taken from attosecond-streaking experiments (Fig. 3c). We compute $j_x(t)$ as the temporal derivative of the field-induced polarization, multiplying it by the effective cross-section, A_{eff}, of the metal–dielectric interfaces confining the active volume of the dielectric. More details are given in the Supplementary Information.

Our computations predict the dependence of

$$Q_P = A_{eff} \int_{-\infty}^{\infty} j_x(t)\, dt$$

on the CEP (Fig. 2a, black dashed line), the peak electric field (Fig. 2b), and the delay between the injection and drive fields for different $F_d(t)$ (Fig. 3) and $F_i(t)$ (Supplementary Fig. 7) waveforms. All the observed dependencies have been excellently reproduced using parameters—defining the band structure and three relevant dipole matrix elements—that we chose once and did not subsequently adjust. The parameter A_{eff} was adjusted to fit the magnitude of the collected charge, and $A_{eff} \approx 5 \times 10^{-12}$ m^2 gave the best agreement with the measurements. This value matches the experimentally estimated metal–dielectric cross-section within an order of magnitude. Hence, our microscopic model predicts our observations both qualitatively and, within an order of magnitude, quantitatively. This quantitative agreement also implies that a significant fraction of the charge separated by the optical currents in the dielectric is transferred to the metal leads, in

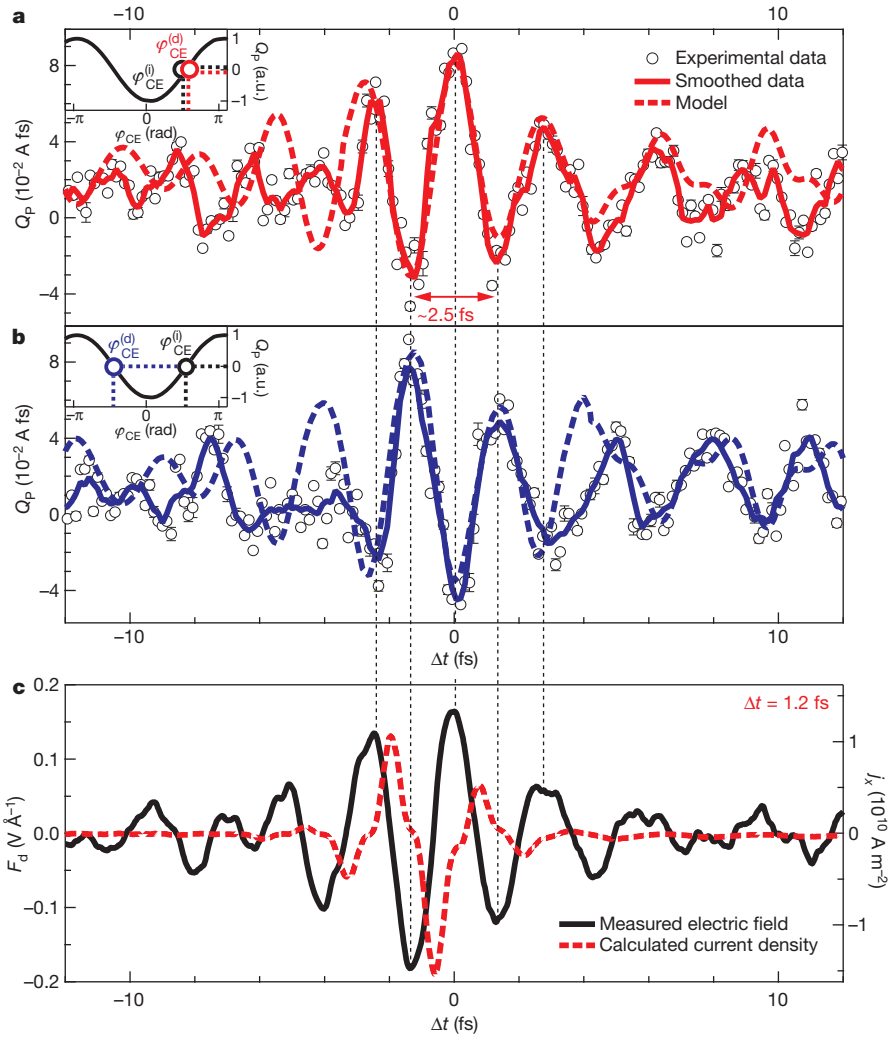

Figure 3 | Subfemtosecond control of electric current with the electric field of light. a, **b**, Transferred charge, Q_P, versus delay, Δt, between the injection ($F_i(t)$) and drive ($F_d(t)$) fields, with parameters as described in the text. For $\Delta t < 0$, $F_d(t)$ precedes $F_i(t)$. The CE phases of the injection and drive fields, $\varphi_{CE}^{(i)}$ and $\varphi_{CE}^{(d)}$ respectively, are set such that Q_P induced independently by any of the two fields vanishes (insets). The experimental data shown were recorded under identical conditions except for $\varphi_{CE}^{(d)}$, which is shifted by π between the two measurements (compare the insets). The experimental data (circles) represent an average of several consecutively acquired values at a given Δt value. The error bars are the respective standard deviations. The solid lines correspond to the smoothed data obtained by averaging over adjacent points. The dashed lines show the prediction of our microscopic quantum mechanical model. Data from our model have been multiplied by the effective cross-section, A_{eff}, of the metal–dielectric interfaces confining the active volume of the dielectric (main text). The slightly asymmetric polarity of the experimental signal could be due to the non-zero residual current for each individual pulse. The dependence of the current on Δt demonstrates that the charge-carrier generation takes place predominantly in the silica medium and that electrons of the gold electrodes, which are not sensitive to the component of the field parallel to the metal–insulator interface, that is, $F_i(t)$, do not contribute to the optically injected current. **c**, Real-time optical electric field of the visible/near-infrared pulses retrieved from attosecond-streaking measurements[24] (solid black line), which were performed under identical laser conditions. The magnitude of the field is normalized to the strength of the drive pulse, $F_d(t)$, used in the photocurrent experiment. The red dashed curve shows the time-dependent current density, $j_x(t)$, as calculated from our quantum mechanical model for $\Delta t = 1.2$ fs. The vertical black dashed lines provide a guide to the eye for comparing the temporal evolution of the measured electronic signal with that of the drive electric field.

line with the predictions of a theoretical study of optically induced currents in a single-molecule nanojunction[10] (Supplementary Information, section 3.4).

The calculated $j_x(t)$ in Fig. 3c and Supplementary Fig. 3 reveals ultrafast turn-on and turn-off behaviour, allowed by the extremely wideband energy spectrum of the dielectric. This predicted temporal behaviour enables us to evaluate the peak current density from our measurements. With a maximum value of $Q_P(\Delta t)$ on the order of 0.1 A fs (Fig. 3a, b) and A_{eff} as specified above, our experimental data yield a transferred charge density of the order of 10^{10} A fs m^{-2}. Given that the duration of the current density pulse is of the order of 1 fs (see $j_x(t)$ in Figs 3c and Supplementary Fig. 3), we estimate a peak current density perpendicular to the electrodes of $J_x \approx 10^{10}$ A m^{-2}, driven by a peak field amplitude of $F_0^{(d)} \approx 0.2 \times 10^{10}$ V m^{-1}. We may now introduce an effective electrical conductivity at optical frequencies as $\sigma_{eff}(\omega_L) = J_x / F_0^{(d)} \approx 5\ \Omega^{-1}\,\mathrm{m}^{-1}$, which exceeds the static d.c. conductivity of amorphous silica, $\sigma_{a\text{-}SiO_2} < 10^{-18}\ \Omega^{-1}\,\mathrm{m}^{-1}$, by more than 18 orders of magnitude.

Our microscopic theory correctly predicts the field-induced increase in polarizability that is responsible for the observed current, but does not provide intuitive insight into its origin. We suggest, with reference to a detailed discussion in the Supplementary Information, that this field-enhanced polarizability can be qualitatively interpreted in terms of the dynamic formation of Wannier–Stark states[25–28] localized at a certain site, l, of the lattice along the direction of the applied field, F, with an energy of $E_l = E_n - eaFl$ (e is the electron charge, a is

the lattice constant and E_n is the band offset) in the adiabatic limit (Fig. 1b). For high fields, $F > 1\,\mathrm{V\,Å^{-1}}$, the eigenenergies of the Wannier–Stark states from the valence band and conduction band that reside at neighbouring lattice sites $|l_v\rangle$ and $|l_c\rangle$ become equal; see the avoided crossing and anticrossing of the respective purple and green plots of energy against field the inset of Fig. 1b. For increasing field strength, adiabatic passage of such an anticrossing via Zener-type tunnelling[17] may occur with a significant probability (Fig. 1b inset, dashed arrow), emptying a valence band state. The resultant unoccupied valence band states give rise to strong visible/near-infrared single-photon resonances within the valence band (Fig. 1b inset, red arrow). The emergence of these resonances directly implies a strong transient polarizability[29,30].

This field-induced transformation is predicted to be reversible and highly nonlinear (as suggested by the resultant $j_x(t)$ in Fig. 3c and Supplementary Fig. 3). The consequence is a sub-cycle increase in the polarizability of the system, which leads to an asymmetric charge displacement along the field vector: the averaging of the current to zero that is inherent in linear processes is eliminated. Consequently, net charge accumulations of opposite sign—dependent on the waveform (Fig. 2) or on the delay between injection and driving fields (Fig. 3)—form at the opposite facets of the dielectric and transfer to the electrodes.

Our experiments reveal an ultrafast 'turning on' of the measured current. At the same time, they do not provide direct evidence for the similarly fast 'turning off' predicted by our theory. A proof of the ultrafast turn-off behaviour of the underlying field-induced nonlinear polarization and conduction band population was provided by recent time-resolved absorption and reflection experiments[31]. This suggests that conductivity and, consequently, current can be switched on and off in a dielectric using optical fields on a timescale of less than, or of the order of, 1 fs, and that this can be done without incurring much dissipation. This operation cycle is similar to that occurring in a field-effect transistor, but is fundamentally more energy efficient: when switching, the field-effect transistor dissipates by electron–hole recombination all energy stored in it, whereas the dielectric in our experiment returns almost all stored energy to the injection field. These possibilities may have ramifications for overcoming the speed limits of semiconductor electronics. In the shorter term, our work holds promise for the development of a solid-state device for direct sampling of electric transients with bandwidths extending to optical frequencies.

METHODS SUMMARY

Source of strong ultrashort optical waveforms. A customized titanium–sapphire chirped-pulse amplifier produces linearly polarized, visible/near-infrared laser pulses with controllable φ_{CE}, a pulse energy of ~400 μJ and a repetition rate of 3 kHz. The ultrabroad spectrum of the laser spans the 450–1,100-nm spectral range, supporting a sub-4-fs pulse duration (full width at half maximum of the intensity temporal profile), which corresponds to a ~1.5-cycle pulse at the carrier wavelength of ~750 nm. The laser pulses can be focused onto the investigated solid-state system such that the cycle-averaged peak intensity reaches $10^{14}\,\mathrm{W\,cm^{-2}}$ (see Supplementary Fig. 2 for properties of the laser).

Photoactive metal–dielectric nanocircuit. The photoactive circuit on which the experiments have been performed consists of a metal–dielectric–metal nanojunction. This structure is fabricated by cleaving amorphous SiO_2 (Crystec GmbH) and coating the adjacent surfaces of the atomically sharp cleaved silica edge with ~50 nm of gold evaporated at grazing incidence. We obtain regular, straight, metal electrodes isolated from each other by dielectric nanoscale trenches with widths of the order of ~50 nm. No voltage bias is applied to the electrodes during the experiment. The junction is coated with a supplementary sputtered silica nanofilm such that the metal electrodes are embedded in a homogeneous silica matrix. See Supplementary Information for more details on the sample structure and experimental set-up. Identical measurements were made on samples composed of cleaved monocrystalline SiO_2(001) (Crystec GmhH) and on flat, ~500-nm gold–SiO_2–gold nanogaps. Both yielded results very similar to those reported in this work, but it was possible to distinguish possible effects arising from the lack of long-range order in the amorphous insulator and from local plasmonic resonances at the metal–dielectric interface. These points are discussed in Supplementary Information.

Detection scheme for the optically induced φ_{CE}-dependent electric signal. In this work, we present experimental data on the φ_{CE}-dependent component of the optically generated electronic signals in the circuit. We isolate the electric current induced by the electric field of the optical waveform from the φ_{CE}-independent contributions (for example electric currents caused by photo-ionization of gold due to imbalanced irradiation of the electrodes). The observable of interest is filtered by synchronizing the pulse train from the chirped-pulse amplifier in such a way that two consecutive ultrashort light bursts have a φ_{CE}-change of π. This results in a modulation of φ_{CE} at half the repetition rate of the pulse train. The optically generated electronic signal in the nanocircuit is measured using a current–voltage converter with a variable high gain and a bandwidth supporting the laser pulse train. The φ_{CE}-dependent component of the current is extracted with a lock-in amplifier locked at the φ_{CE} modulation frequency. The presented data correspond to experiments performed in ambient atmosphere at ~20 °C. We carried out identical measurements in vacuum, yielding the same results.

Received 20 December 2011; accepted 31 August 2012.
Published online 5 December 2012.

1. Kahng, D. Electric field controlled semiconductor device. US patent 3,102 230 (1963).
2. Taur, Y. & Ning, T. H. *Fundamentals of modern VLSI devices* (Cambridge Univ. Press, 1998).
3. Liou, J. J. & Schwierz, F. *Modern Microwave Transistors: Theory, Design and Performance* (Wiley-Interscience, 2003).
4. Caulfield, H. J. & Dolev, S. Why future supercomputing requires optics. *Nature Photon.* **4,** 261–263 (2010).
5. Schwierz, F. & Liou, J. J. RF transistors: recent developments and roadmap toward terahertz applications. *Solid-State Electron.* **51,** 1079–1091 (2007).
6. Deal, W. R. *et al.* Low noise amplification at 0.67 THz using 30 nm InP HEMTs. *IEEE Microw. Wirel. Compon. Lett.* **21,** 368–370 (2011).
7. Kurizki, G., Shapiro, M. & Brumer, P. Phase-coherent control of photocurrent directionality in semiconductors. *Phys. Rev. B* **39,** 3435–3437 (1989).
8. Atanasov, R., Hache, A., Hughes, J. L. P., van Driel, H. M. & Sipe, J. E. Coherent control of photocurrent generation in bulk semiconductors. *Phys. Rev. Lett.* **76,** 1703–1706 (1996).
9. Prechtel, L. *et al.* Time-resolved picosecond photocurrents in contacted carbon nanotubes. *Nano Lett.* **11,** 269–272 (2011).
10. Franco, I., Shapiro, M. & Brumer, P. Robust ultrafast currents in molecular wires through stark shifts. *Phys. Rev. Lett.* **99,** 126802 (2007).
11. Valley, G. C. Photonic analog-to-digital converters. *Opt. Express* **15,** 1955–1982 (2007).
12. Nagatsuma, T. Photonic measurement technologies for high-speed electronics. *Meas. Sci. Technol.* **13,** 1655–1663 (2002).
13. Auston, D. H. Picosecond optoelectronic switching and gating in silicon. *Appl. Phys. Lett.* **26,** 101–103 (1975).
14. Auston, D. H. Ultrafast optoelectronics. *Top. Appl. Phys.* **60,** 183–233 (1988).
15. Shimosato, H., Ashida, M., Itoh, T., Saito, S. & Sakai, K. in *Ultrafast Optics V* (eds Watanabe, S. & Midorikawa, K.) 317–323 (Springer Ser. Opt. 132, Springer, 2007).
16. Katzenellenbogen, N. & Grischkowsky, D. Efficient generation of 380 fs pulses of THz radiation by ultrafast laser-pulse excitation of a biased metal-semiconductor interface. *Appl. Phys. Lett.* **58,** 222–224 (1991).
17. Zener, C. A theory of the electrical breakdown of solid dielectrics. *Proc. R. Soc. Lond. A* **145,** 523–529 (1934).
18. Rethfeld, B. Free-electron generation in laser-irradiated dielectrics. *Phys. Rev. B* **73,** 035101 (2006).
19. Jones, S. C., Braunlich, P., Casper, R. T., Shen, X. A. & Kelly, P. Recent progress on laser-induced modifications and intrinsic bulk damage of wide-gap optical-materials. *Opt. Eng.* **28,** 1039–1068 (1989).
20. Lenzner, M. *et al.* Femtosecond optical breakdown in dielectrics. *Phys. Rev. Lett.* **80,** 4076–4079 (1998).
21. Schwierz, F., Wong, H. & Liou, J. J. *Nanometer CMOS* (Pan Stanford, 2010).
22. Koslowski, T., Kob, W. & Vollmayr, K. Numerical study of the electronic structure of amorphous silica. *Phys. Rev. B* **56,** 9469–9476 (1997).
23. Xu, L. *et al.* Route to phase control of ultrashort light pulses. *Opt. Lett.* **21,** 2008–2010 (1996).
24. Kienberger, R. *et al.* Atomic transient recorder. *Nature* **427,** 817–821 (2004).
25. Wannier, G. H. Wave functions and effective Hamiltonian for Bloch electrons in an electric field. *Phys. Rev.* **117,** 432–439 (1960).
26. Bleuse, J., Bastard, G. & Voisin, P. Electric-field-induced localization and oscillatory electro-optical properties of semiconductor superlattices. *Phys. Rev. Lett.* **60,** 220–223 (1988).
27. Mendez, E. E., Agulló-Rueda, F. & Hong, J. M. Stark localization in GaAs-GaAlAs superlattices under an electric field. *Phys. Rev. Lett.* **60,** 2426–2429 (1988).
28. Bar-Joseph, I. *et al.* Room-temperature electroabsorption and switching in a GaAs/AlGaAs superlattice. *Appl. Phys. Lett.* **55,** 340–342 (1989).
29. Durach, M., Rusina, A., Kling, M. F. & Stockman, M. I. Metallization of nanofilms in strong adiabatic electric fields. *Phys. Rev. Lett.* **105,** 086803 (2010).
30. Durach, M., Rusina, A., Kling, M. F. & Stockman, M. I. Predicted ultrafast dynamic metallization of dielectric nanofilms by strong single-cycle optical fields. *Phys. Rev. Lett.* **107,** 086602 (2011).
31. Schultze, M. *et al.* Controlling dielectrics with the electric field of light. *Nature* doi:10.1038/nature11720 (this issue).

Supplementary Information is available in the online version of the paper.

Acknowledgements We thank P. Altpeter and Y. Deng for technical support and discussions, and we thank the Munich-Centre for Advanced Photonics for financial support. A.S. acknowledges the Alexander von Humboldt Foundation and the Swiss National Science Foundation. N.K. acknowledges the Alexander von Humboldt Foundation. The work of M.I.S. and V.A. was supported by the Chemical Sciences, Biosciences and Geosciences Division (grant no. DEFG02-01ER15213) and by the Materials Sciences and Engineering Division (grant no. DE-FG02-11ER46789) of the Office of the Basic Energy Sciences, Office of Science, US Department of Energy. R.K. acknowledges an ERC Starting Grant.

Author Contributions A.S., R.K., R.E. and F.K. designed and supervised the experiments. A.S., T.P.-C., D.G., S.M., J.R. and J.V.B. participated in sample design and fabrication. A.S., T.P.-C., N.K., D.G., S.M., M.S. and S.H. performed the measurements. A.S., N.K., V.A., M.K., V.S.Y. and M.I.S. took part in the theoretical modelling. A.S., T.P.-C., N.K., R.K., R.E., V.S.Y. and F.K. analysed and interpreted the experimental data. All authors discussed the results and contributed to the final manuscript.

Author Information Reprints and permissions information is available at www.nature.com/reprints. The authors declare no competing financial interests. Readers are welcome to comment on the online version of the paper. Correspondence and requests for materials should be addressed to A.S. (aschiffr@phas.ubc.ca), M.I.S. (mstockman@gsu.edu) or F.K. (ferenc.krausz@mpq.mpg.de).